

# Measuring the Virial Factor in SDSS DR5 Quasars with Redshifted $H\beta$ and Fe II Broad Emission Lines

H. T. Liu<sup>1,2,3\*</sup>, Hai-Cheng Feng<sup>1,2,3,4</sup>, Sha-Sha Li<sup>1,2,3</sup>, and J. M. Bai<sup>1,2,3</sup>

## ABSTRACT

Under the hypothesis of gravitational redshift induced by the central supermassive black hole, and based on line widths and shifts of redward shifted  $H\beta$  and Fe II broad emission lines for a sample of 1973  $z < 0.8$  SDSS DR5 quasars, we measured the virial factor in determining supermassive black hole masses, usually estimated by the reverberation mapping (RM) method or the relevant secondary methods. The virial factor had been believed to be from the geometric effect of broad-line region. The measured virial factor of Fe II is larger than that of  $H\beta$  for 98% of these quasars. The virial factor is very different from object to object and for different emission lines. For most of these quasars, the virial factor of  $H\beta$  is larger than these averages that were usually used in determining the masses of black holes. There are three positive correlations among the measured virial factor of  $H\beta$ , dimensionless accretion rate and Fe II/ $H\beta$  line ratio. A positive three-dimensional correlation is found among these three quantities, and this correlation indicates that the virial factor is likely dominated by the dimensionless accretion rate and metallicity. A negative correlation is found between the redward shift of  $H\beta$  and the scaled size of broad-line region radius in units of the gravitational radius of black hole. This negative correlation will be expected naturally if the redward shift of  $H\beta$  is mainly from the gravity of black hole. Radiation pressure from accretion disk may be a significant contributor to the virial factor.

*Subject headings:* Active galactic nuclei (16) – Black hole physics (159) – Emission line galaxies (459) – Quasars (1319) – Supermassive black holes (1663)

---

<sup>1</sup>Yunnan Observatories, Chinese Academy of Sciences, 396 Yangfangwang, Guandu District, Kunming, 650216, People's Republic of China

<sup>2</sup>Key Laboratory for the Structure and Evolution of Celestial Objects, Chinese Academy of Sciences, Kunming 650011, Yunnan, People's Republic of China

<sup>3</sup>Center for Astronomical Mega-Science, Chinese Academy of Sciences, 20A Datun Road, Chaoyang District, Beijing, 100012, People's Republic of China

<sup>4</sup>University of Chinese Academy of Sciences, Beijing 100049, People's Republic of China

\*Corresponding author: H. T. Liu, htliu@ynao.ac.cn

## 1. INTRODUCTION

Mass,  $M_{\bullet}$ , is an important fundamental parameter of black hole, and reliable measurement of  $M_{\bullet}$  always will be a key issue of black hole related researches, such as the researches and understanding of the formation, growth, and evolution of the black holes in the Universe and the coevolution debates of supermassive black holes (SMBHs) and host galaxies (e.g., Kormendy & Ho 2013). Assuming virialized motion of clouds in broad-line region (BLR), the reverberation mapping (RM) method or the relevant secondary methods based on single-epoch spectra were widely used to measure  $M_{\bullet}$  by a RM black hole mass  $M_{\text{RM}} = f v_{\text{FWHM}}^2 r_{\text{BLR}} / G$  for active galactic nuclei (AGNs), where  $f$  is the virial factor,  $v_{\text{FWHM}}$  is full width at half maximum of broad emission line,  $r_{\text{BLR}}$  is radius of BLR, and  $G$  is the gravitational constant (e.g., Peterson et al. 2004).  $f$  is commonly considered the main source of uncertainty in  $M_{\text{RM}}$ . If the line width  $v_{\text{FWHM}}$  is replaced with  $\sigma_{\text{line}}$ , the second moment of emission line,  $f$  becomes  $f_{\sigma}$ . The virial factor had been believed to be induced by the geometric effect of BLR. Based on the photoionization assumption (e.g., Blandford & McKee 1982; Peterson 1993),  $r_{\text{BLR}} = \tau_{\text{ob}} c / (1 + z)$ , where  $c$  is the speed of light,  $z$  is redshift of source, and  $\tau_{\text{ob}}$  is the time lag observed between the broad-line and continuum variations. For non-RM AGNs with single-epoch spectra,  $r_{\text{BLR}}$  can be estimated with the radius–luminosity relation, i.e., the empirical  $r_{\text{BLR}}-L(5100 \text{ \AA})$  relation for  $\text{H}\beta$  emission line, established on the basis of the RM AGNs, where  $L(5100 \text{ \AA})$  is AGN continuum luminosity at rest frame wavelength  $5100 \text{ \AA}$  (e.g., Kaspi et al. 2000; Bentz et al. 2013; Du et al. 2018b; Du & Wang 2019; Yu et al. 2020).

The RM observation researches have been made for more than 100 AGNs over the last several decades (e.g., Kaspi & Netzer 1999; Kaspi et al. 2000, 2007; Bentz et al. 2006, 2010; Peterson et al. 2005; Denney et al. 2010; Barth et al. 2011, 2015; Haas et al. 2011; Pozo Nuñez et al. 2012; Du et al. 2014, 2015, 2016, 2018a,b; Pei et al. 2014, 2017; Wang et al. 2014; Hu et al. 2015; Lu et al. 2016; Xiao et al. 2018a,b; Zhang et al. 2019; Feng et al. 2021a,b). RM surveys have been run, such as the OzDES AGN spectroscopic RM project (King et al. 2015; Hoormann et al. 2019) and the Sloan Digital Sky Survey (SDSS) spectroscopic RM project (Shen et al. 2015a,b, 2016, 2019; Grier et al. 2017). The single-epoch spectrum was widely used to estimate  $M_{\text{RM}}$  for the SDSS quasars (e.g., Hu et al. 2008; Liu et al. 2019) and the high- $z$  quasars (e.g., Willott et al. 2010; Wu et al. 2015; Wang et al. 2019). However, the virial factor is very uncertain due to the unclear kinematics and geometry of BLR (e.g., Peterson et al. 2004; Woo et al. 2015). Radiation pressure of accretion disk has significant influences on the BLR clouds and the dynamics of clouds (e.g., Marconi et al. 2008; Netzer & Marziani 2010; Krause et al. 2011, 2012; Naddaf et al. 2021). The dynamics of clouds can determine the three dimensional geometry of BLR (Naddaf et al. 2021). Thus, radiation pressure may be a contributor to the virial factor. Radiation pressure was not considered in estimating  $M_{\text{RM}}$ . Averages of  $f \approx 1$  and/or  $f_{\sigma} \approx 5$  were derived based on the  $M_{\bullet} - \sigma_{*}$  relation for the low- $z$  inactive and quiescent galaxies, where  $\sigma_{*}$  is stellar velocity dispersion of galaxy bulge (e.g., Tremaine et al. 2002; Onken et al. 2004; Piotrovich et al. 2015; Woo et al. 2015).  $f \approx 1$  and/or  $f_{\sigma} \approx 5$  were usually used to estimate  $M_{\text{RM}}$  by the RM and/or the single-epoch spectra of AGNs. Thus, measuring  $f$  and/or  $f_{\sigma}$  independently by a new method for individual AGNs is necessary

and important to understand the physics of the BLR and the issues related to black hole masses.

Liu et al. (2017) proposed a new method to measure  $f$  based on the widths and shifts of redward shifted broad emission lines for the RM AGNs. The Fe III  $\lambda\lambda$  2039–2113 UV line blend arises from an inner region of the BLR (Mediavilla et al. 2018), and a lot of evidence shows that the UV blend originates close to the SMBH (e.g., Mediavilla & Jiménez-Vicente 2021). Large values of  $f$  are obtained from the widths and redward shifts of these UV blends, and an average of  $\langle f_{\text{FeIII}} \rangle = 14.3 \pm 2.4$  is derived for 10 lensed quasars with a mean Eddington ratio of  $\sim 0.8$  (Mediavilla et al. 2020). This average value is much larger than the widely accepted one of  $f \approx 1$ . However, the origin of redward shifts of broad emission lines are unclear, because the origin of broad emission lines in AGNs is not yet clear (e.g., Wang et al. 2017). A tight correlation between broadening and redward shift of the Fe III  $\lambda\lambda$  2039–2113 blend for quasars in the BOSS survey supports the gravitational interpretation of its redward shift (Mediavilla et al. 2018). Alternative explanations, such as inflow, will need additional physics to explain the observed trend between broadening and redshift (Mediavilla et al. 2018). The redward shifts of the root mean square profiles of broad emission lines with respect to narrow emission lines and the BLR radii in Mrk 110 follow the gravitational redshift prediction (see Fig. 3 in Kollatschny 2003). The velocity-resolved time lags of H $\beta$  broad emission line for Mrk 50 and SBS 1518+593 show characteristic of Keplerian disk or virialized motion (Barth et al. 2011; Du et al. 2018a). A sign of the gravitational redshift  $z_g$  was found in a statistical sense for broad H $\beta$  in the single-epoch spectra of SDSS DR 7 quasars (Tremaine et al. 2014).

Hu et al. (2008) suggested that inflow may generate the redward shifts of broad emission lines. Absorption lines that are redshifted with respect to the quasar’s systemic velocity are an unambiguous signature of inflow (Rubin 2017). Inflow generates the redward shifts of broad absorption lines relative to the quasar’s systemic velocity determined from narrow emission lines, and the broad absorption and emission lines may be from different gas regions due to their distinct velocities (Zhou et al. 2019). Redward shifts of broad emission lines of H $\gamma$ , H $\beta$ , and He I lines for Mrk 817 seemingly have an origin of outflow that is denoted by the redward asymmetric velocity-resolved lag profiles of these lines (Lu et al. 2021). However, the redward shifts of broad emission lines are commonly believed to be from inflow that will lead to the blueward asymmetric velocity-resolved lag profiles. This discrepancy implies that the redward shifts of broad emission lines do not originate from inflow. For each RM observation cycle of NGC 5548, Lu et al. (2016) found that the variations of average 5100 Å luminosity lead the changes of  $r_{\text{BLR}}$  by  $\tau_{\text{T-L}} = 2.35$  yr, which is consistent with a dynamical timescale of  $t_{\text{BLR}} \approx 2.10$  yr for the BLR, and they obtained that the BLR could be jointly controlled by the radiation pressure of accretion disk and the central black hole gravity. Krause et al. (2011) found that stable orbits of clouds in BLR exist for very sub-Keplerian rotation, for which the radiation pressure force contributes substantially to the force budget. Thus, the radiation pressure force might result in significant influence on the virial factor. In this work, SDSS DR5 quasars with redward shifted H $\beta$  and Fe II broad emission lines (see Table 2 in Hu et al. 2008) are used to investigate the virial factor, relations between the virial factor and other physical

quantities for these quasars, and the origin of the redward shift of H $\beta$  broad emission line.

The structure is as follows. Section 2 presents method. Section 3 describes sample selection. Section 4 presents discussion and conclusions. Throughout this paper, we assume a standard cosmology with  $H_0 = 70 \text{ km s}^{-1} \text{ Mpc}^{-1}$ ,  $\Omega_M = 0.3$ , and  $\Omega_\Lambda = 0.7$  (Spergel et al. 2007).

## 2. METHOD

A BLR cloud is subject to gravity of black hole,  $F_g$ , and radiation pressure force,  $F_r$ , due to central continuum radiation. Under the resultant force of  $F_t = F_g + F_r$ , the total mechanical energy and angular momentum are conserved for the BLR clouds because  $F_g$  and  $F_r$  are central forces. Under various assumptions,  $F_r$  can be calculated for more than hundreds of thousands of lines, with detailed photoionization, radiative transfer, and energy balance calculations (e.g., Dannen et al. 2019). In principle,  $M_\bullet$  could be estimated by the BLR cloud motions as the numerical calculation methods give  $F_r$ . However, the various assumptions may significantly influence the reliability of  $F_r$ . Especially, many unknown physical parameters are likely various for different AGNs. Thus, a new method was proposed to measure  $f$  when avoiding the numerical calculation of  $F_r$  (Liu et al. 2017).

The virial factor formula in Liu et al. (2017) was derived from the Schwarzschild metric for a static cloud. In fact, the BLR clouds are not static, e.g., in the virialized motion. The gravitational redshift in the Schwarzschild space-time for the BLR clouds can be expressed as (see Equation 12 in Chakraborty & Bhattacharyya 2018)

$$z_g = \left(1 - \frac{3GM_\bullet}{c^2 r_{\text{BLR}}}\right)^{-1/2} - 1, \quad (1)$$

where the gravitational and transverse Doppler shifts are taken into account.  $M_\bullet$  is estimated as

$$M_\bullet = \frac{1}{3}G^{-1}c^2 r_{\text{BLR}} \left[1 - (1 + z_g)^{-2}\right], \quad (2)$$

and the first order approximation is

$$M_\bullet = \frac{2}{3}G^{-1}c^2 z_g r_{\text{BLR}}, \quad (3)$$

as  $z_g \ll 1$  or  $r_g/r_{\text{BLR}} \ll 1$  for optical broad emission lines (the gravitational radius  $r_g = GM_\bullet/c^2$ ).

Here, Equation (3) is the same as Equation (3) of Mediavilla et al. (2018), in which the weak field limit of the Schwarzschild metric was assumed. At the optical BLR scales, the Schwarzschild metric is valid and matches the weak field limit. Equation (1) is valid for a disklike BLR (see Chakraborty & Bhattacharyya 2018). The disklike BLR is preferred by some RM observations of AGNs, e.g., NGC 3516 (e.g., Denney et al. 2010; Feng et al. 2021a), and the VLTI instrument GRAVITY observations of quasar 3C 273 (GRAVITY Collaboration et al. 2018). For rapidly rotating BLR clouds, the relativistic beaming effect can give rise to a profile asymmetry with an enhanced

blue side in broad emission lines, i.e., blueshifts of broad emission lines (Mediavilla & Inertis 1989). Thus, the relativistic beaming effect should be neglected for the redward shifted broad emission lines, which should be dominated by the gravitational redshift and transverse Doppler effects. The factor of 2/3 in Equation (3) results from correcting the transverse Doppler shift, which is essentially that the moving clock becomes slower. The factor of 2/3 does not appear in the formulas used to estimate  $M_{\bullet}$  in Kollatschny (2003) and Liu et al. (2017), because they did not consider the transverse Doppler shift. If  $M_{\bullet}$  estimated with Equation (2) is equal to  $M_{\text{RM}}$ , we have the virial factor

$$f = \frac{1}{3} \frac{c^2}{v_{\text{FWHM}}^2} \left[ 1 - (1 + z_g)^{-2} \right]. \quad (4)$$

If  $v_{\text{FWHM}}$  is replaced with  $\sigma_{\text{line}}$ ,  $f$  becomes  $f_{\sigma}$ .

Because  $r_{\text{BLR}} \gg r_g$  for optical broad emission lines, Equation (1) can give the multi-broad-line approach of measuring  $M_{\bullet}$  as

$$M_{\bullet} \cong \frac{2}{3} G^{-1} c^2 \Delta z_{i,j} \left( \frac{1}{r_{\text{BLR},i}} - \frac{1}{r_{\text{BLR},j}} \right)^{-1}, \quad (5)$$

where  $\Delta z_{i,j} = z_i - z_j = z_{g,i} - z_{g,j}$  is the redshift difference between the broad lines  $i$  and  $j$  with the relevant BLR radius  $r_{\text{BLR},i}$  and  $r_{\text{BLR},j}$ . Here, Equations (2), (3), (4), and (5) have the factor of 2/3 more than Equations (4), (5), (9), and (7) derived in Liu et al. (2017), respectively. The reliability of the redward shift method was confirmed by the consistent masses estimated from their Equations (4) and (7) based on 4 broad emission lines for Mrk 110 (Liu et al. 2017). Thus, Equations (2) and (5) in this work can also give consistent black hole masses for Mrk 110. The RM observations of multi broad emission lines for AGNs might further test the reliability of this method, based on Equations (2) and (5). Hereafter,  $M_{\text{RM}}$  denotes  $M_{\bullet}$  measured with the RM method and/or the relevant secondary methods, and  $f_g$  denotes the virial factor that comes from the geometric effect of BLR.

### 3. SAMPLE SELECTION

Hu et al. (2008) reported a systematical investigation of optical Fe II emission in a large sample of 4037  $z < 0.8$  quasars selected from the SDSS DR5, for which they had developed and tested a detailed line-fitting technique, taking into account the complex continuum and narrow and broad emission line spectra. The line widths and redward velocity shifts of the Fe II and H $\beta$  spectra are given in Table 2 of Hu et al. (2008). On the basis of  $\Delta v - \sigma(\Delta v) > 0$ , where  $\Delta v$  is the redward velocity shift for the H $\beta$  and Fe II broad emission lines (i.e.,  $\Delta v > 0$ ), and  $\sigma(\Delta v)$  is the error of  $\Delta v$ , 1973 quasars are selected out of these 4037 quasars as our sample. This selection condition makes sure that the velocity shift is larger than zero within  $1\sigma$  uncertainties. If  $\Delta v - \sigma(\Delta v) \leq 0$ , it is possible that the velocity shift is redshift, blueshift, or no-shift. Thus, the redward velocity shift seems much less reliable if  $\Delta v - \sigma(\Delta v) \leq 0$ , and this selection condition of  $\Delta v - \sigma(\Delta v) > 0$  seems reasonable.

Because the empirical  $r_{\text{BLR}}-L(5100 \text{ \AA})$  relation is established for broad emission line  $\text{H}\beta$ , the relevant researches of the virial factor are made mainly with the broad  $\text{H}\beta$  line. Some physical quantities are taken from Table 2 in Hu et al. (2008), including the cosmological redshift of source:  $z$ ,  $v_{\text{FWHM}}(\text{H}\beta)$ ,  $\sigma_{\text{line}}(\text{H}\beta)$ , the redward velocity shift of broad  $\text{H}\beta$ :  $\Delta v(\text{H}\beta)$ ,  $v_{\text{FWHM}}(\text{Fe II})$ ,  $\Delta v(\text{Fe II})$ ,  $L(5100 \text{ \AA})$ , the black hole mass, the Eddington ratio, and the line ratio of Fe II to  $\text{H}\beta$ . The bolometric luminosity in the Eddington ratio was estimated in Hu et al. (2008) using  $L_{\text{bol}} = 9L(5100 \text{ \AA})$  (Kaspi et al. 2000). The details of sample are listed in Table 1. The virial factor is estimated by Equation (4), and the relevant values for the  $\text{H}\beta$  and Fe II broad emission lines are listed in Table 1. The dimensionless accretion rate  $\dot{\mathcal{M}}_{f_g} = L_{\text{bol}}/L_{\text{Edd}}(f_g)/\eta$ , where  $\eta$  is the efficiency of converting rest-mass energy to radiation,  $L_{\text{bol}}$  is the bolometric luminosity,  $L_{\text{Edd}}$  is the Eddington luminosity,  $f_g = 1$  for  $v_{\text{FWHM}}$ , and  $f_g = 5.5$  for  $\sigma_{\text{line}}$ . Here, we adopt  $\eta = 0.038$  (Du et al. 2015).

Table 1. The relevant parameters for 1973 quasars in SDSS DR5

Designation	$z$	$\frac{v_{\text{FWHM}}(\text{H}\beta)}{\text{km s}^{-1}}$	$\frac{\sigma_{\text{H}\beta}}{\text{km s}^{-1}}$	$\frac{\Delta v(\text{H}\beta)}{\text{km s}^{-1}}$	$\frac{v_{\text{FWHM}}(\text{FeII})}{\text{km s}^{-1}}$	$\frac{\Delta v(\text{FeII})}{\text{km s}^{-1}}$	$\log L$	$\frac{M_{\text{RM}}}{10^7 M_{\odot}}$	$\frac{L_{\text{bol}}}{L_{\text{Edd}}}$	$R_{\text{Fe}}$	$f(\text{H}\beta)$	$f_{\sigma}(\text{H}\beta)$	$f(\text{Fe II})$	$\log \mathcal{M}_{f_{\text{g}}}$	$\frac{r_{\text{BLR}}}{r_{\text{g}}}$
(1)	(2)	(3)	(4)	(5)	(6)	(7)	(8)	(9)	(10)	(11)	(12)	(13)	(14)	(15)	(16)
000011.96+000225.3	0.4784	3135.8±62.6	1893.5	542.3±35.4	1898.6±74.1	387.6±38.4	44.74	28.1	0.140	1.318	11.0±0.8	30.2±3.7	21.5±2.7	0.57	4535.0
000111.19 - 002011.5	0.5173	3666.5±125.3	2267.1	486.9 ±66.3	2496.5±406.2	1082.1±156.9	44.60	32.2	0.088	0.609	7.2±1.1	18.9±3.2	34.5±15.9	0.37	3159.8
000131.42+144610.6	0.5309	5054.5±306.4	2299.3	481.9±103.9	3359.2±658.1	1595.2±214.5	44.44	25.8	0.077	0.640	3.8±0.9	18.2±4.4	28.0±17.1	0.31	3069.8
...	...	...	...	...	...	...	...	...	...	...	...	...	...	...	...

Note. — Column 1: object name; Column 2: redshift; Column 3:  $v_{\text{FWHM}}$  of H $\beta$  broad emission line; Column 4:  $\sigma_{\text{line}}$  of H $\beta$  broad emission line; Column 5: the redward velocity shift of H $\beta$ ; Column 6:  $v_{\text{FWHM}}$  of Fe II broad emission line; Column 7: the redward velocity shift of Fe II; Column 8: logarithm of  $L(5100 \text{ \AA})$  in units of  $\text{erg s}^{-1}$ ; Column 9: the black hole mass; Column 10: the Eddington ratio; Column 11: the Fe II/H $\beta$  line ratio; Column 12: the virial factor estimated from  $v_{\text{FWHM}}$  of H $\beta$ ; Column 13: the virial factor estimated from  $\sigma_{\text{line}}$  of H $\beta$ ; Column 14: the virial factor estimated from  $v_{\text{FWHM}}$  of Fe II; Column 15: logarithm of  $\mathcal{M}_{f_{\text{g}}=5.5}$ ; Column 16:  $r_{\text{BLR}}$  in units of  $r_{\text{g}}$ , where  $r_{\text{BLR}} = 22.3L_{44}^{0.69}$  light-days with  $L_{44} = L(5100 \text{ \AA})/(10^{44} \text{ erg s}^{-1})$ . Columns 2–11 are taken from Table 2 of Hu et al. (2008) or converted from the relevant quantities in Table 2 of Hu et al. (2008).

(This table is available in its entirety in machine-readable form.)

#### 4. ANALYSIS AND RESULTS

The Spearman’s rank correlation test shows that the virial factor is positively correlated with the dimensionless accretion rate  $\dot{\mathcal{M}}_{f_g=5.5}$  for these 1973 quasars (see Figure 1 and Table 2). The virial factor and  $\dot{\mathcal{M}}_{f_g=5.5}$  are related to the line width, and this line width dependency may result in a false correlation between them. The partial correlation analysis gives a confidence level of 99.99% for the positive correlation of  $\log f_\sigma - \log \dot{\mathcal{M}}_{f_g=5.5}$  when excluding the dependence on the line width  $\sigma_{\text{line}}$ . Since the virial factor may be affected by  $F_r$ , it is possible that the virial factor is correlated with  $L(5100 \text{ \AA})$ . So, we analyze the virial factor and  $L(5100 \text{ \AA})$ , and find no correlation between them (see Figure 2). Thus, the positive correlation exists between the virial factor and  $\dot{\mathcal{M}}_{f_g=5.5}$ . This positive correlation is qualitatively consistent with the logical expectation when the overall effect of  $F_r$  on the BLR clouds is taken into account to estimate  $M_{\text{RM}}$ . In addition,  $f_\sigma > f_g = 5.5$  and  $f > f_g = 1$  for  $\text{H}\beta$  in most of quasars (see Figure 1).

In order to test the gravitational origin of the redward velocity shift of broad emission line, we compare  $\Delta v(\text{H}\beta)$  to  $r_{\text{BLR}}/r_g(f_g = 5.5)$ , the BLR radius in units of the gravitational radius of black hole. The Spearman’s rank correlation test shows negative correlation between the velocity shift and  $r_{\text{BLR}}/r_g(f_g = 5.5)$  (see Figure 3a and Table 2). This negative correlation is qualitatively consistent with the expectation when  $\Delta v(\text{H}\beta)$  is mainly from the gravity of the central black hole. The values of  $r_{\text{BLR}}/r_g(f_g = 5.5)$  in Figure 3a are estimated based on the uncorrected  $M_{\text{RM}}(f_g = 5.5)$ . However,  $M_{\text{RM}}(f_g = 5.5)$  could not be corrected individually for each quasar due to the absence of the different individual virial factor that is independent of  $\Delta v(\text{H}\beta)$ . The overall correction of  $M_{\text{RM}}(f_g = 5.5)$  for these 1973 quasars can be made by a factor of 3.4 derived from  $f_g = 5.5$  and an average of  $f_\sigma = 18.5$  presented in Figure 1a (see Figure 3b). This overall correction is equivalent to the overall parallel shift of the data in Figure 3a. Figure 3b shows that the negative correlation expectation is basically consistent with the trend between  $\Delta v(\text{H}\beta)$  and the corrected  $r_{\text{BLR}}/r_g(f_g = 5.5)$ . This indicates that  $\Delta v(\text{H}\beta)$  is dominated by the gravity of the central black hole. In addition,  $r_g/r_{\text{BLR}} \lesssim 0.01 \ll 1$  for the  $x$ -axis values in Figures 3a and 3b and the values of  $r_g/r_{\text{BLR}}$  corrected by  $f_\sigma$  in Table 1. At these optical BLR scales of quasars, the Schwarzschild metric is valid and still matches the weak field limit. The RM researches of AGNs may shed light on the origin of  $\Delta v(\text{H}\beta)$ , and the relevant discussion is presented in the next section.

The virial factor of Fe II is larger than that of  $\text{H}\beta$  for 98% of these quasars (see Figure 4). Also, Figure 4 shows that the virial factor is very different from object to object and for different emission lines. If the stratified photoionization found for broad emission lines is prevalent in AGNs, the optimized photoionization zones in BLRs will be different for different lines. For clouds at a given radius,  $F_r$  is the resultant force from the different ions with negligible drift velocities between the gas constituents within these clouds, which generate a prominent broad emission line component. Also, the typical size of cloud of BLR is much less than the extent of BLR. So,  $F_r$  on clouds at the different radius is different, thus potentially resulting in different virial factors. Fe II may be from a region outside the BLR of  $\text{H}\beta$ , i.e.,  $r_{\text{BLR}}(\text{Fe II}) > r_{\text{BLR}}(\text{H}\beta)$  (e.g., Hu et al. 2008, and references therein). The RM of quasar 3C 273 showed  $r_{\text{BLR}}(\text{Fe II}) > r_{\text{BLR}}(\text{H}\beta)$  (Zhang et al. 2019). For broad



emission lines with different  $r_{\text{BLR}}$ , there will be  $f \propto r_{\text{BLR}}^\alpha$  ( $\alpha > 0$ ) as  $F_r$  is considered and the BLR clouds are in the virialized motion for a given AGN (Liu et al. 2017). If  $r_{\text{BLR}}(\text{Fe II}) > r_{\text{BLR}}(\text{H}\beta)$  and  $f \propto r_{\text{BLR}}^\alpha$ , it will be expected that the measured virial factor of Fe II is larger than that of H $\beta$  for most of quasars in our sample.

Netzer & Trakhtenbrot (2007) have suggested that  $R_{\text{FeII}}$  is a BLR metallicity indicator for SDSS type 1 AGNs. Panda et al. (2018, 2019) have suggested that  $R_{\text{FeII}}$  is associated with the BLR metallicity.  $R_{\text{FeII}}$  increases with the increasing metallicity. The BLR metallicity can influence  $F_r$  due to the line-driven force dominated by the metallic elements (e.g., Ferland et al. 2009; Dannen et al. 2019). Thus,  $R_{\text{FeII}}$  may influence the virial factor. Three positive correlations exist among  $f_\sigma$ ,  $R_{\text{FeII}}$ , and  $\mathcal{M}_{f_g=5.5}$  (see Table 2 and Figure 5). Since three correlations exist among them, there should be a correlation like as  $f_\sigma(\mathcal{M}_{f_g=5.5}, R_{\text{FeII}})$ . In fact, there is a positive correlation at the confidence level of  $> 99.99\%$ ,  $\log f_\sigma = -0.41 + 0.11 \log \mathcal{M}_{f_g=5.5} + 0.28 \log R_{\text{FeII}}$ . Thus,  $f_\sigma$  is dominated by  $R_{\text{FeII}}$  and  $\mathcal{M}_{f_g=5.5}$  (or the Eddington ratio). This should be easily understood that  $F_r$  exerted on the BLR clouds will be larger as the BLR metallicity is higher and/or the radiation of accretion disk is stronger. Thus, the observed envelope delineating the data should be a consequence of physical effects, such as the Doppler effects, the gravitational redshift, and the line-driven force, which depend on the black hole mass, the bolometric luminosity of the black hole, and the BLR metallicity.

## 5. DISCUSSION AND CONCLUSIONS

As  $z_g \ll 1$ , Equation (4) can give for  $\sigma_{\text{line}}$ ,  $f_\sigma$  and  $z_g = \Delta v/c$

$$\log\left(\frac{\sigma_{\text{line}}}{c}\right)^2 = -\log\left(\frac{3}{2}f_\sigma\right) + \log\left(\frac{\Delta v}{c}\right), \quad (6)$$

which is similar to Equation (6) in Mediavilla et al. (2018), where a tight correlation was found between the widths and redward shifts of the Fe III $\lambda\lambda$  2039–2113 blend for their quasars, and this correlation supports the gravitational interpretation of the Fe III $\lambda\lambda$  2039–2113 redward shifts. The Spearman’s rank correlation test shows a positive correlation between the line width and velocity shift of the H $\beta$  line for these 1973 quasars (see Table 2). A series of lines based on Equation (6) with different  $f_\sigma$  are compared to the observational data points (see Figure 6). From top to bottom, the corresponding  $f_\sigma$  increases. Because of the co-dependence between the Eddington ratio, dimensionless accretion rate and  $\sigma_{\text{line}}$ , the large ranges of the former two quantities may lead to the large span in the direction roughly perpendicular to these lines (see Figure 6). Also, the metallicity difference of BLR might decrease correlations in Figure 1. Micro-turbulence within the BLR clouds can act as an apparent metallicity controller for the Fe II, and the reduction in the value of the metallicity can be up to a factor of ten for the Fe II/H $\beta$  line ratio  $R_{\text{FeII}}$  when the micro-turbulence is invoked (Panda 2021). In addition, spectral simulations show that  $R_{\text{FeII}}$  depends clearly on cloud column density (e.g., Ferland et al. 2009). The combination of the column

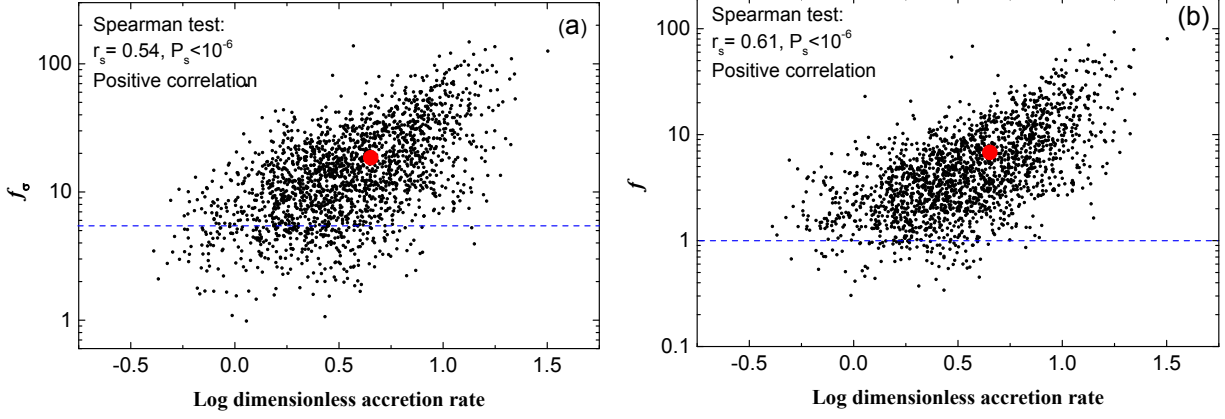


Fig. 1.— Panel (a):  $H\beta$ - $\sigma_{\text{line}}$ -based  $f_{\sigma}$  vs.  $\dot{M}_{f_g=5.5}$ . Spearman test shows a positive correlation between these two physical quantities, which have averages corresponding to the red solid circle. The dashed line denotes  $f_g = 5.5$  for  $\sigma_{\text{line}}$ . Panel (b):  $H\beta$ - $v_{\text{FWHM}}$ -based  $f$  vs.  $\dot{M}_{f_g=5.5}$ . Spearman test shows a positive correlation between these two physical quantities, which have averages corresponding to the red solid circle. The dashed line denotes  $f_g = 1$  for  $v_{\text{FWHM}}$ .

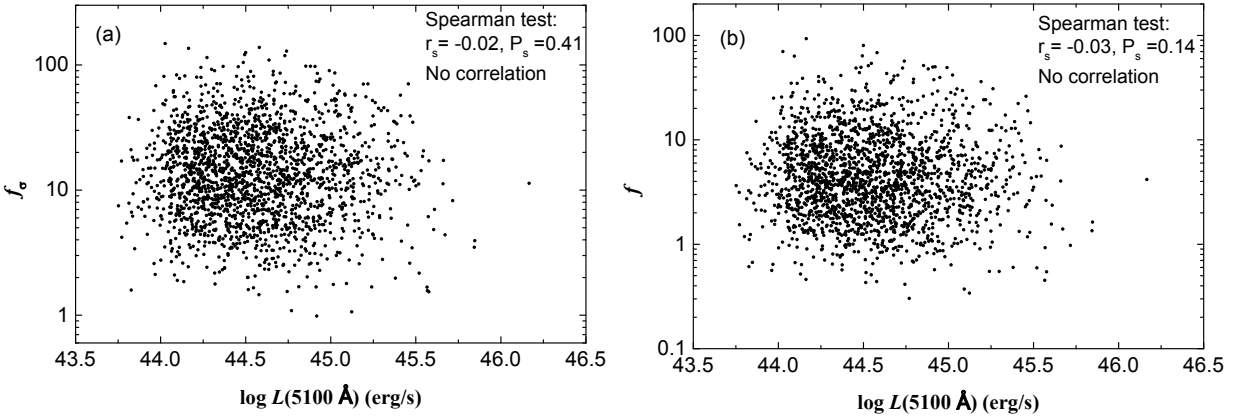


Fig. 2.— Panel (a):  $H\beta$ - $\sigma_{\text{line}}$ -based  $f_{\sigma}$  vs.  $L(5100 \text{ \AA})$  and Panel (b):  $H\beta$ - $v_{\text{FWHM}}$ -based  $f$  vs.  $L(5100 \text{ \AA})$ . Spearman test shows no correlation.

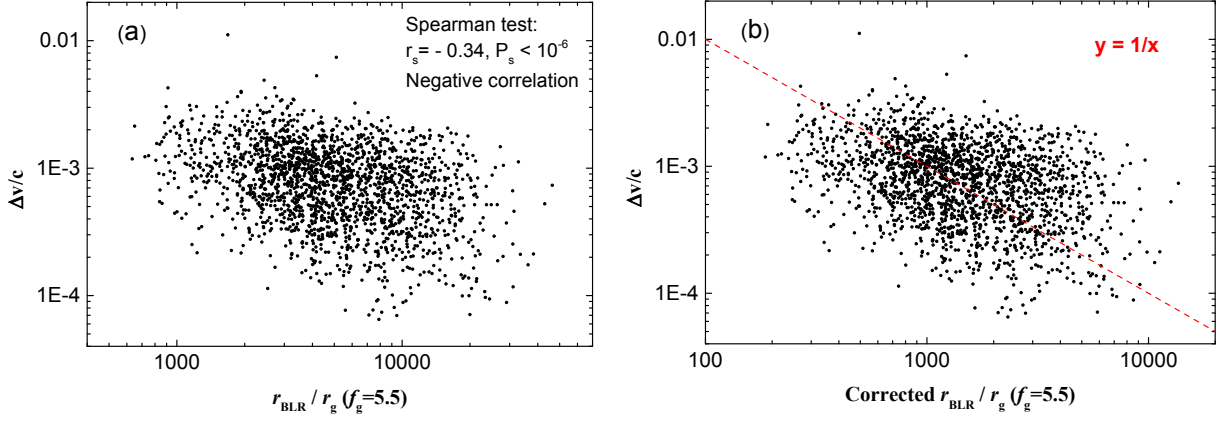


Fig. 3.— Panel (a): H $\beta$  velocity shift  $\Delta v/c$  vs.  $r_{\text{BLR}}/r_g (f_g = 5.5)$ . Spearman test shows negative correlation between these two physical quantities. Panel (b): H $\beta$  velocity shift  $\Delta v/c$  vs.  $r_{\text{BLR}}/r_g (f_g = 5.5)$  corrected by a factor of 3.4.

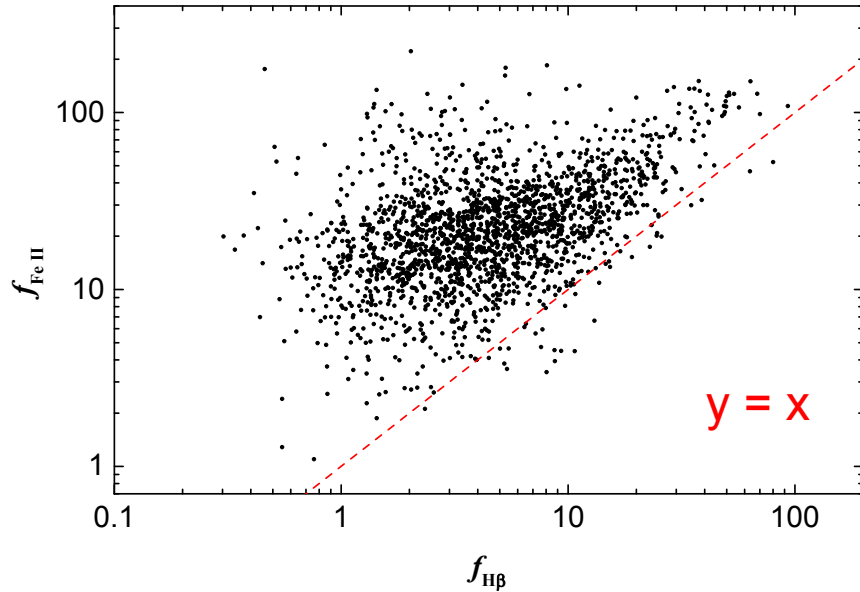


Fig. 4.—  $f$  for Fe II vs.  $f$  for H $\beta$  based on  $v_{\text{FWHM}}$ .

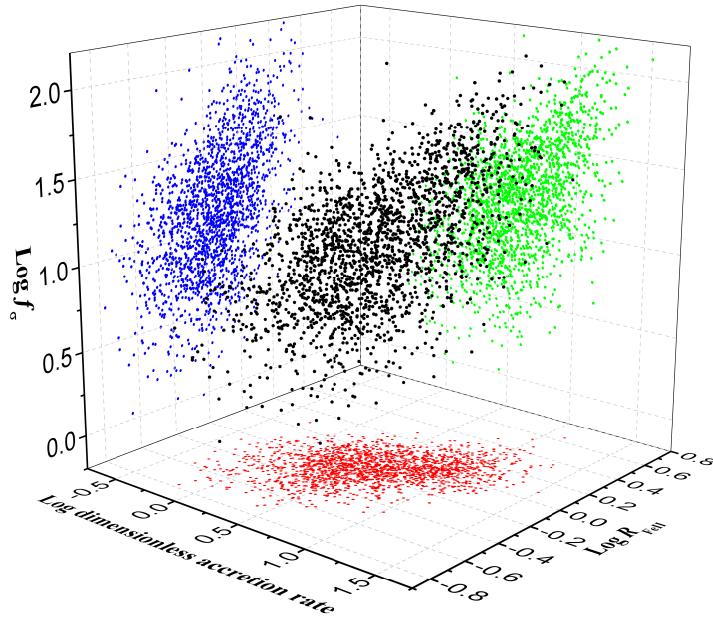


Fig. 5.— 3D plot of  $\dot{M}_{f_g=5.5}$ ,  $R_{\text{FeII}}$ , and  $f_\sigma$  (black points). Color points correspond to  $XY$ ,  $XZ$ , and  $YZ$  projections of black points.

density, metallicity and internal physical processes may further decrease these correlations in Figure 1.

The shifts of broad emission lines may originate from the non-virialized BLR, e.g., outflows or inflows. However, gas outflows can generate the blueshifts of emission lines, e.g., narrow forbidden lines [O III] (e.g., Condon et al. 1985; Shen & Ho 2014) and broad emission line C IV (e.g., Wang et al. 2011). The [O III] emission lines can be decomposed into two components: a narrow Gaussian component and a blueshifted/blue-skewed broad component. According to Hu et al. (2008), the shifts of broad emission lines are derived with respect to the narrow Gaussian component of [O III] $\lambda$  5007. Thus, the shifts of broad emission lines taken from Table 2 in Hu et al. (2008) are not influenced by these blueshifted/blue-skewed broad components of [O III]. The outflows in AGNs can be pushed by the line-driven force (e.g., Dannen et al. 2019; Dyda & Proga 2018; Mas-Ribas & Mauland 2019), and accretion disk winds driven by the line force have the increasing velocity with roughly decreasing acceleration from the black hole to the far (Nomura et al. 2020). Observations show the various outflows at accretion disk scales, the BLR scales, the NLR scales and the kpc scales, driven by  $F_r$  from AGNs (Kang & Woo 2018; Meena et al. 2021; Singha et al. 2021). Thus,  $F_r$  is prevalent, and might contribute to the force budget for inflow, e.g.,  $F_r$  decelerates inflow (Ferland et al. 2009). RM observations of PG 0026+129 indicate a decelerating inflow towards the black hole if  $\Delta v$  originates from inflow. If the decelerating inflow is prevalent,  $\Delta v$  will increase with the increasing  $r_{\text{BLR}}/r_g (f_g = 5.5)$ , and this expectation is not consistent with the trend found in Figure 3. Thus, the inflow seems not to be the origin of  $\Delta v(\text{H}\beta)$ .

It was believed that inflow generates the redward shifted broad emission lines with the blueward asymmetric velocity-resolved lag maps obtained in RM observations, and outflow generates the blueward shifted broad emission lines with the redward asymmetric lag maps. However, the asymmetric lag maps and shifts of broad emission lines for AGNs usually differ from the expectations of inflow, such as 3C 273 (e.g., Zhang et al. 2019), PG 0026+129 (Hu et al. 2020), NGC 3516 (e.g., Denney et al. 2010; Feng et al. 2021a), and NGC 2617 (e.g., Feng et al. 2021b). The redward shifted broad emission lines with the blueward asymmetric lag maps might be generated by an elliptical disklike BLR or a circular disklike BLR plus a spiral armlike BLR (Feng et al. 2021a). Eccentricities and orientations of cloud orbits significantly influence full two-dimensional transfer function (2DTF) of a single disklike BLR (see Figure 3 in Kovačević et al. 2020), and the redward shifted broad emission lines with various lag maps may originate from the clouds in virialized motion with various asymmetric responses in 2DTF. Virialized BLRs are suggested by the symmetric lag maps of redward shifted broad emission lines for SBS 1116+583A (Bentz et al. 2009), Mrk 50 (Barth et al. 2011), and SBS 1518+593 (Du et al. 2018a). Therefore, the redward shifted broad emission lines in AGNs do not necessarily originate from inflow.

These 2485 quasars with  $\Delta v(\text{H}\beta) > 0$  in Table 2 of Hu et al. (2008) have a median of  $\Delta v(\text{H}\beta) = 190 \text{ km s}^{-1}$  with a typical error of  $55 \text{ km s}^{-1}$ , and an average and standard deviation of  $\langle \Delta v \rangle(\text{H}\beta) = 238 \pm 67 \text{ km s}^{-1}$ . 1973 quasars in our sample have  $\Delta v(\text{H}\beta) = 242 \pm 52 \text{ km s}^{-1}$  and  $\langle \Delta v \rangle(\text{H}\beta) = 281 \pm 63 \text{ km s}^{-1}$ . Considering uncertainties, these distributions of  $\Delta v(\text{H}\beta)$  do not seem obviously

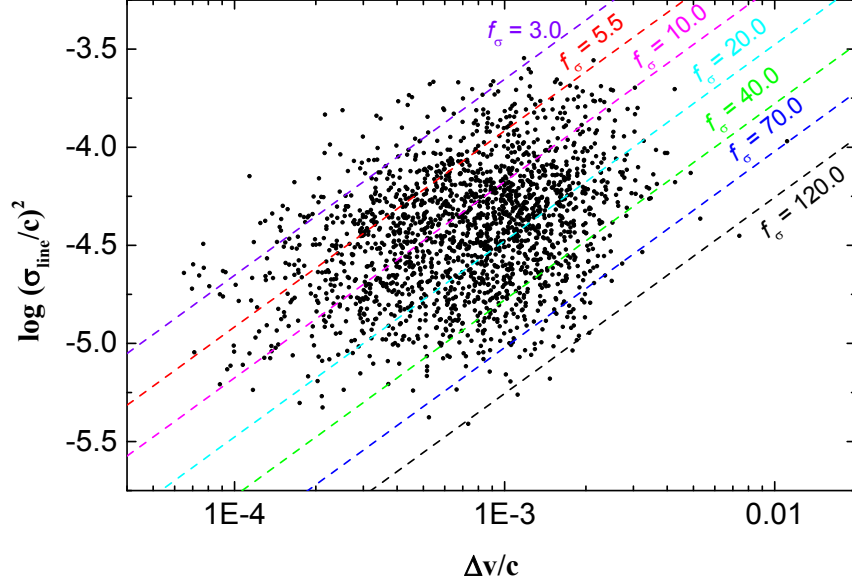


Fig. 6.—  $\log(\sigma_{\text{line}}/c)^2$  vs.  $\Delta v/c$  for the  $\text{H}\beta$  line. The values labelled on the dashed lines represent  $f_\sigma$  in Equation (6).

Table 2. Spearman’s rank analysis results.

X	Y	$r_s$	$P_s$
$\mathcal{M}_{f_g=5.5}$ or $L_{\text{bol}}/L_{\text{Edd}}$	$f_\sigma$	0.54	$< 10^{-6}$
$\mathcal{M}_{f_g=5.5}$ or $L_{\text{bol}}/L_{\text{Edd}}$	$f$	0.61	$< 10^{-6}$
$L(5100\text{\AA})$	$f_\sigma$	-0.02	0.41
$L(5100\text{\AA})$	$f$	-0.03	0.14
$r_{\text{BLR}}/r_g(f_g = 5.5)$	$\Delta v/c$	-0.34	$< 10^{-6}$
$\Delta v/c$	$(\sigma_{\text{line}}/c)^2$	0.34	$< 10^{-6}$
$R(\text{Fe II}/\text{H}\beta)$	$f_\sigma$	0.43	$< 10^{-6}$
$\mathcal{M}_{f_g=5.5}$ or $L_{\text{bol}}/L_{\text{Edd}}$	$R(\text{Fe II}/\text{H}\beta)$	0.54	$< 10^{-6}$

Note. — X and Y are the relevant quantities presented in Figures 1–6. The SPEAR (Press et al. 1992) gives  $r_s$  and  $P_s$  (the Spearman’s rank correlation coefficient and the p-value of hypothesis test, respectively).

different. The relevant distributions of  $\Delta v(\text{H}\beta)$  are presented in Figure 7a. Sources with smaller  $\Delta v(\text{H}\beta)$  are more likely excluded by  $\Delta v - \sigma(\Delta v) > 0$ , which means the relative error of  $\Delta v$  is smaller than 1. The relative error distributions in Figure 7b for the 1973 and 2485 quasar samples show that the relative error is more likely larger for the smaller  $\Delta v$ . Correlation analyses for 2485 quasars show, at the confidence level of  $> 99.99\%$ , three positive correlations among  $f_\sigma$ ,  $R_{\text{FeII}}$  and  $\dot{\mathcal{M}}_{f_g=5.5}$ , a positive correlation like as  $f_\sigma(\dot{\mathcal{M}}_{f_g=5.5}, R_{\text{FeII}})$ , and a negative correlation between  $\Delta v(\text{H}\beta)$  and  $r_{\text{BLR}}/r_g(f_g = 5.5)$ . These results indicate that correlations found for 1973 quasars do not originate from the selection effect, i.e.,  $\Delta v - \sigma(\Delta v) > 0$  will not result in illusive correlations, though this condition will make  $\Delta v$  larger for the selected quasars. The fraction of blueshifted broad line  $\text{H}\beta$  with  $\Delta v + 3\sigma(\Delta v) < 0$  is about 14% for quasars in Hu et al. (2008), and these blueshifted quasars may be explained by additional blueshift of a kinematic origin arising from radial motion, e.g., outflows. Outflows seem exist even if AGNs are during their low-flux states (e.g., Mehdipour et al. 2022). Larger quasar sample, e.g., SDSS DR7 quasars in Liu et al. (2019) who gave the detailed parameters of spectra, will be used in the next work.

The radiative efficiency is closely related to a black hole spin, but it is difficult to measure the spin of the black hole in AGN. Usually, the Eddington ratio is regarded as a proxy of accretion rate of black hole. Even though these correlations of the dimensionless accretion rate with the other physical quantities are likely influenced by the unknown real individual value of radiative efficiency, there are still correlations of the Eddington ratio with these physical quantities, because only a difference of 0.038 exists between  $\dot{\mathcal{M}}_{f_g=5.5}$  and  $L_{\text{bol}}/L_{\text{Edd}}$  in Table 1. Based on  $L_{\text{bol}}$  and the mass accretion rate, Davis & Laor (2011) determined  $\eta$  for a sample of 80 Palomar—Green quasars, and found a strong correlation of  $\eta = 0.089M_8^{0.52}$ , where  $M_8$  is the black hole mass in units of  $10^8 M_\odot$ . In order to test the influence of a fixed radiative efficiency  $\eta = 0.038$ , this empirical relation is used to estimate  $\eta$ . Correlation analyses are made for those quantities in Figures 1 and 5 with  $\dot{\mathcal{M}}_{f_g=5.5}$  to be re-estimated by  $L_{\text{bol}}/L_{\text{Edd}}$  in Table 1 and the estimated  $\eta$ . There are still correlations very similar to those found in Figures 1 and 5 as using these new dimensionless accretion rates (see Figures 8 and 9). A positive correlation,  $\log f_\sigma = -0.24 + 0.09 \log \dot{\mathcal{M}}_{f_g=5.5} + 0.21 \log R_{\text{FeII}}$ , exists at the confidence level of  $> 99.99\%$  (see Figure 9). Thus, these correlations found in this work do not result from using the fixed value of  $\eta = 0.038$ .

Based on the assumption of a gravitational origin for the redward shifts of broad emission lines  $\text{H}\beta$  and  $\text{Fe II}$ , and their widths and redward shifts for a sample of 1973  $z < 0.8$  SDSS DR5 quasars, we measured the virial factor in  $M_{\text{RM}}$ , estimated by the RM method and/or the relevant secondary methods. The measured virial factor contains the overall effect of  $F_r$  from accretion disk radiation and the geometric effect of BLR.  $f_\sigma > 5.5$  and  $f > 1$  for the broad  $\text{H}\beta$  in most quasars (see Figure 1).  $f_{\text{FeII}} > f_{\text{H}\beta}$  for 98% of these 1973 quasars, which is consistent with the deduction from  $r_{\text{BLR}}(\text{Fe II}) > r_{\text{BLR}}(\text{H}\beta)$  and  $f \propto r_{\text{BLR}}^\alpha$  ( $\alpha > 0$ ). The virial factor is very different from object to object and for different emission lines (see Figure 4). A series of lines, based on Equation (6) with different  $f_\sigma$ , basically reproduce the distribution of  $(\sigma_{\text{line}}, \Delta v)$  for the  $\text{H}\beta$  line (see Figure 6), supporting the gravitational interpretation of  $\Delta v$  for the  $\text{H}\beta$  line. There are three positive

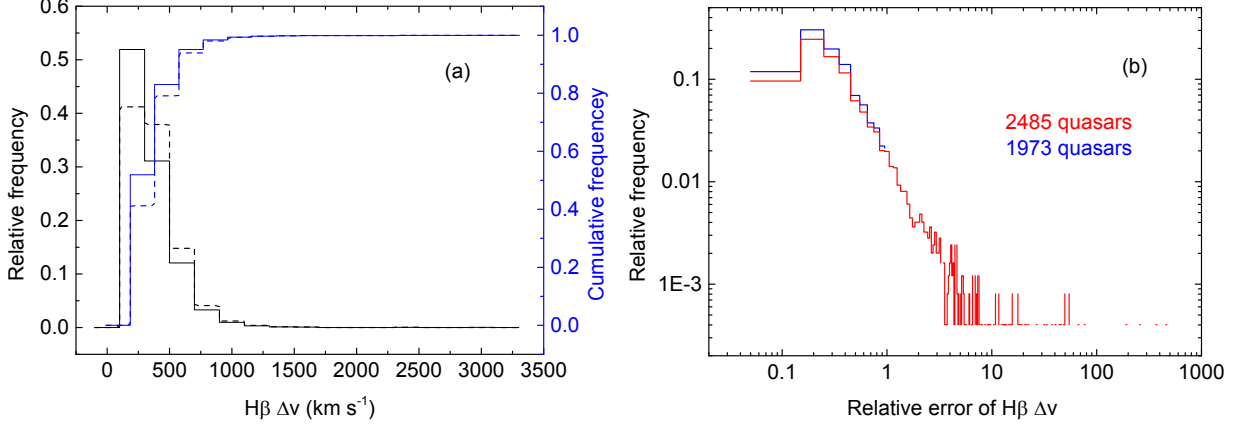


Fig. 7.— Distributions of  $\Delta v(\text{H}\beta)$  and its relative error. Panel (a): the solid lines are the distributions for 2485 quasars with  $\Delta v(\text{H}\beta) > 0$  in Hu et al. (2008). The dashed lines are the distributions for 1973 quasars in our sample. Panel (b): distributions of the relative error of  $\Delta v(\text{H}\beta)$ .

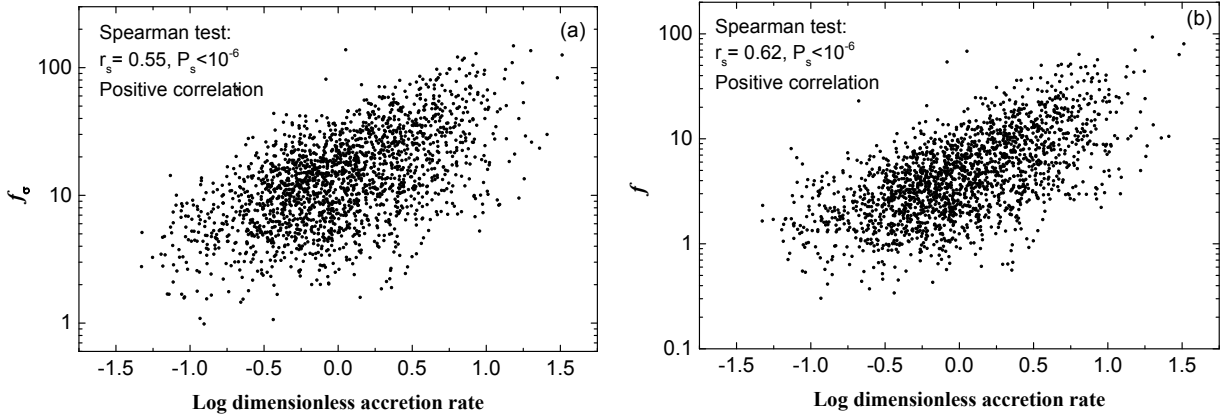


Fig. 8.— Panel (a):  $\text{H}\beta\text{-}\sigma_{\text{line}}$ -based  $f_{\sigma}$  vs.  $\dot{\mathcal{M}}_{f_g=5.5}$ . Spearman test shows a positive correlation between these two physical quantities. Panel (b):  $\text{H}\beta\text{-}v_{\text{FWHM}}$ -based  $f$  vs.  $\dot{\mathcal{M}}_{f_g=5.5}$ . Spearman test shows a positive correlation between these two physical quantities.  $\dot{\mathcal{M}}_{f_g=5.5}$  is the value estimated by  $\eta = 0.089M_{\text{g}}^{0.52}$  rather than  $\eta = 0.038$ .



correlations among  $f_{\sigma}(\text{H}\beta)$ ,  $\mathcal{M}_{f_g=5.5}$  and  $R_{\text{FeII}}$ . A correlation,  $\log f_{\sigma} = -0.41 + 0.11 \log \mathcal{M}_{f_g=5.5} + 0.28 \log R_{\text{FeII}}$ , indicates that the virial factor is dominated by  $\mathcal{M}_{f_g=5.5}$  and metallicity, which will influence  $F_{\text{T}}$  on the BLR clouds.  $\Delta v(\text{H}\beta)$  is anti-correlated with  $r_{\text{BLR}}/r_g(f_g = 5.5)$ , supporting the gravitational origin of the redward shift of  $\text{H}\beta$ . Our results indicate that  $F_{\text{T}}$  may be an important contributor to the virial factor, and the redward shifted broad emission lines show the potential of measuring the virial factor.

We are very grateful to the anonymous referees for constructive comments leading to significant improvement of this paper. We thank the helpful discussions of Prof. J R Mao. We thank the financial support of the National Natural Science Foundation of China (NSFC; grant No. 11991051), and we acknowledge the science research grants from the China Manned Space Project with NO. CMS-CSST-2021-A06.

### ORCID iDs

H. T. Liu <https://orcid.org/0000-0002-2153-3688>

Hai-Cheng Feng <https://orcid.org/0000-0002-1530-2680>

### REFERENCES

- Barth, A. J., Pancoast, A., Thorman, S. J., et al. 2011, *ApJ*, 743, L4
- Barth, A. J., Bennert, V. N., Canalizo, G., et al. 2015, *ApJS*, 217, 26
- Bentz, M. C., Denney, K. D., Cackett, E. M., et al. 2006, *ApJ*, 651, 775
- Bentz, M. C., Walsh, J. L., Barth, A. J., et al. 2009, *ApJ*, 705, 199
- Bentz, M. C., Walsh, J. L., Barth, A. J., et al. 2010, *ApJ*, 716, 993
- Bentz, M. C., Denney, K. D., Grier, C. J., et al. 2013, *ApJ*, 767, 149
- Blandford, R. D., & McKee, C. F. 1982, *ApJ*, 255, 419
- Chakraborty, C., & Bhattacharyya, S. 2018, *Phys. Rev. D*, 98, 3021
- Condon, J. J., Hutchings, J. B., & Gower, A. C. 1985, *AJ*, 90, 1642
- Dannen, R. C., Proga, D., Kallman, T. R., & Waters, T. 2019, *ApJ*, 882, 99
- Davis, S. W., & Laor, A. 2011, *ApJ*, 728, 98
- Denney, K. D., Peterson, B. M., Pogge, R. W., et al. 2010, *ApJ*, 721, 715

- (SEAMBH Collaboration) Du, P., Hu, C., Lu, K. X., et al. 2014, *ApJ*, 782, 45
- (SEAMBH Collaboration) Du, P., Hu, C., Lu, K. X., et al. 2015, *ApJ*, 806, 22
- (SEAMBH Collaboration) Du, P., Lu, K. X., Hu, C., et al. 2016, *ApJ*, 820, 27
- (MAHA Collaboration) Du, P., Brotherton, M. S., Wang, K., et al. 2018a, *ApJ*, 869, 142
- (SEAMBH Collaboration) Du, P., Zhang, Z. X., Wang, K., et al. 2018b, *ApJ*, 856, 6
- Du, P., & Wang, J. M. 2019, *ApJ*, 886, 42
- Dyda, S., & Proga, D. 2018, *MNRAS*, 481, 5263
- Feng, H. C., Hu, C., Li, S. S., et al. 2021a, *ApJ*, 909, 18
- Feng, H. C., Liu, H. T., Bai, J. M., et al. 2021b, *ApJ*, 912, 92
- Ferland, G. J., Hu, C., Wang, J. M., et al. 2009, *ApJL*, 707, L82
- Grier, C. J., Trump, J. R., Shen, Y., et al. 2017, *ApJ*, 851, 21
- Haas, M., Chini, R., Ramolla, M., et al. 2011, *A&A*, 535, A73
- Hoormann, J. K., Martini, P., Davis, T. M., et al. 2019, *MNRAS*, 487, 3650
- Hu, C., Wang, J. M., Ho, L. C., et al. 2008, *ApJ*, 687, 78
- (SEAMBH Collaboration) Hu, C., Du, P., Lu, K. X., et al. 2015, *ApJ*, 804, 138
- (SEAMBH Collaboration) Hu, C., Li, S. S., Guo, W. J., et al. 2020, *ApJ*, 905, 75
- Kang, D., & Woo, J. H. 2018, *ApJ*, 864, 124
- Kaspi, S., & Netzer, H. 1999, *ApJ*, 524, 71
- Kaspi, S., Smith, P. S., Netzer, H., et al. 2000, *ApJ*, 533, 631
- Kaspi, S., Brandt, W. N., Maoz, D., et al. 2007, *ApJ*, 659, 997
- King, A. L., Martini, P., Davis, T. M., et al. 2015, *MNRAS*, 453, 1701
- Kollatschny, W. 2003, *A&A*, 412, L61
- Kormendy, J., & Ho, L. C. 2013, *ARA&A*, 51, 511
- Kovačević, A. B., Wang, J.-M., & Popović, L. Č. 2020, *A&A*, 635, A1
- Krause, M., Burkert, A., & Schartmann, M. 2011, *MNRAS*, 411, 550
- Krause, M., Schartmann, M., & Burkert, A. 2012, *MNRAS*, 425, 3172

- Liu, H. T., Feng, H. C., & Bai, J. M. 2017, *MNRAS*, 466, 3323
- Liu, H. Y., Liu, W. J., Dong, X. B., et al. 2019, *ApJS*, 243, 21
- Lu, K. X., Du, P., Hu, C., et al. 2016, *ApJ*, 827, 118
- Lu, K. X., Wang, J. G., Zhang, Z. X., et al. 2021, *ApJ*, 918, 50
- Marconi A. et al. 2008, *ApJ*, 678, 693
- Mas-Ribas, L., & Mauland, R. 2019, *ApJ*, 886, 151
- Mediavilla, E., & Insertis, F. M. 1989, *A&A*, 214, 79
- Mediavilla, E., Jiménez-Vicente, J., Fian, C., et al. 2018, *ApJ*, 862, 104
- Mediavilla, E., Jiménez-vicente, J., Mejía-Restrepo, J., et al. 2020, *ApJ*, 895, 111
- Mediavilla, E., & Jiménez-Vicente, J. 2021, *ApJ*, 914, 112
- Meena, B., Crenshaw, D. M., Schmitt, H. R., et al. 2021, *ApJ*, 916, 31
- Mehdipour, M., Kriss, G. A., Brenneman, L. W., et al. 2022, *ApJ*, 925, 84
- Naddaf, M. H., Czerny, B., & Szczerba, R. 2021, *ApJ*, 920, 30
- Netzer, H. & Marziani, P. 2010, *ApJ*, 724, 318
- Netzer, H., & Trakhtenbrot, B. 2007, *ApJ*, 654, 754
- Nomura, M., Ohsuga, K., & Done, C. 2020, *MNRAS*, 494, 3616
- Onken, C. A., Ferrarese, L., Merritt, D., et al. 2004, *ApJ*, 615, 645
- Panda, S., Czerny, B., Adhikari, T. P., et al. 2018, *ApJ*, 866, 115
- Panda, S., Czerny, B., Done, C., & Kubota, A. 2019, *ApJ*, 875, 133
- Panda, S. 2021, *A&A*, 650, A154
- Pei, L., Barth, A. J., Aldering, G. S., et al. 2014, *ApJ*, 795, 38
- Pei, L., Fausnaugh, M. M., Barth, A. J., et al. 2017, *ApJ*, 837, 131
- Peterson, B. M. 1993, *PASP*, 105, 247
- Peterson, B. M., Ferrarese, L., Gilbert, K. M., et al. 2004, *ApJ*, 613, 682
- Peterson, B. M., Bentz, M. C., Desroches, L. B., et al. 2005, *ApJ*, 632, 799

- Piotrovich, M. Y., Gnedin, Y. N., Silant'ev, N. A., Natsvlshvili, T. M., & Buliga, S. D. 2015, *MNRAS*, 454, 1157
- Pozo Nuñez, F., Ramolla, M., Westhues, C., et al. 2012, *A&A*, 545, A84
- Press W. H., Teukolsky S. A., Vetterling W. T., & Flannery B. P., 1992, *Numerical Recipes*, 2nd edn. Cambridge Univ. Press, Cambridge
- Rubin, K. H. R., in *Gas Accretion onto Galaxies Vol. 430* (eds Fox, A. & Davé, R.), 95 (Springer, 2017)
- Shen, Y., & Ho, L. C. 2014, *Natur.*, 513, 210
- Shen, Y., Brandt, W. N., Dawson, K. S., et al. 2015a, *ApJS*, 216, 4
- Shen, Y., Greene, J. E., Ho, L. C., et al. 2015b, *ApJ*, 805, 96
- Shen, Y., Horne, K., Grier, C. J., et al. 2016, *ApJ*, 818, 30
- Shen, Y., Hall, P. B., Horne, K., et al. 2019, *ApJS*, 241, 34
- Singha, M., O’Dea, C. P., Gordon, Y. A., Lawlor-Forsyth, C., & Baum, S. A., 2021, *ApJ*, 918, 65
- Spergel, D. N., et al. 2007, *ApJS*, 170, 377
- (Gravity Collaboration) Sturm, E., Dexter, J., et al. 2018, *Natur*, 563, 657
- Tremaine, S., Gebhardt, K., Bender, R., et al. 2002, *ApJ*, 574, 740
- Tremaine, S., Shen, Y., Liu, X., & Loeb, A. 2014, *ApJ*, 794, 49
- Wang, F. G., Wang, R., Fan, X. H., et al. 2019, *ApJ*, 880, 2
- Wang, H. Y., Wang, T. G., Zhou, H. Y., et al. 2011, *ApJ*, 738, 85
- (SEAMBH Collaboration) Wang, J. M., Du, P., Hu, C., et al. 2014, *ApJ*, 793, 108
- Wang, J. M., Du, P., Brotherton, M. S., et al. 2017, *Nature Astronomy*, 1, 775
- Willott, C. J., Albert, L., Arzoumanian, D., et al. 2010, *AJ*, 140, 546
- Woo, J. H., Yoon, Y., Park, S., Park, D., & Kim, S. C. 2015, *ApJ*, 801, 38
- Wu, X. B., Wang, F. G., Fan, X. H., et al. 2015, *Natur*, 518, 512
- (SEAMBH Collaboration) Xiao, M., Du, P., Horne, K., et al. 2018a, *ApJ*, 864, 109
- Xiao, M., Du, P., Lu, K. K., et al. 2018b, *ApJL*, 865, L8
- Yu, L. M., Zhao, B. X., Bian, W. H., Wang, C., & Ge, X. 2020, *MNRAS*, 491, 5881

Zhang, Z. X., Du, P., Smith, P. S., et al. 2019, ApJ, 876, 49

Zhou, H. Y., Shi, X. H., Yuan, W. M., et al. 2019, Natur., 573, 83

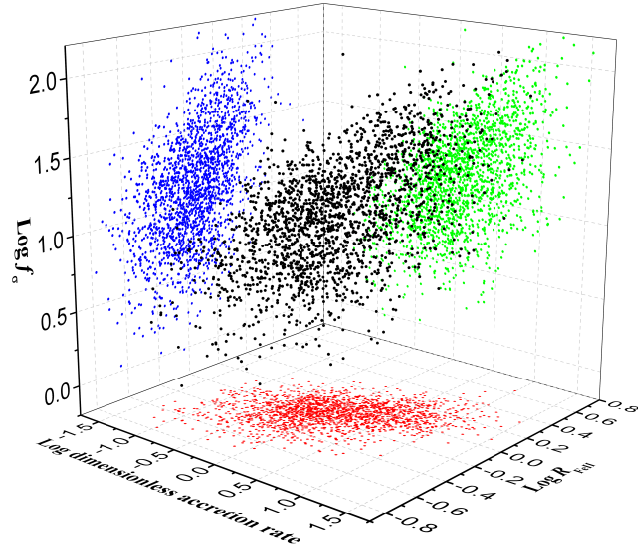


Fig. 9.— 3D plot of  $\dot{\mathcal{M}}_{f_g=5.5}$ ,  $R_{\text{FeII}}$ , and  $f_\sigma$  (black points), where  $\dot{\mathcal{M}}_{f_g=5.5}$  is the value estimated by  $\eta = 0.089M_8^{0.52}$  rather than  $\eta = 0.038$ . Color points correspond to  $XY$ ,  $XZ$ , and  $YZ$  projections of black points.